

Effective Interactions In Neutron-Rich Matter

P. G. Krastev¹, F. Sammarruca², Bao-An Li¹, and A. Worley¹

¹ Texas A&M University-Commerce, Commerce, TX 75429, U.S.A.

² University of Idaho, Moscow, ID 83843, U.S.A.

Abstract. Properties of effective interactions in neutron-rich matter are reflected in the medium's equation of state (EOS), which is a relationship among several state variables. Spin and isospin asymmetries play an important role in the energy balance and could alter the stability conditions of the nuclear EOS. The EOS has far-reaching consequences for numerous nuclear processes in both the terrestrial laboratories and the cosmos. Presently the EOS, especially for neutron-rich matter, is still very uncertain. Heavy-ion reactions provide a unique means to constrain the EOS, particularly the density dependence of the nuclear symmetry energy. On the other hand, microscopic, self-consistent, and parameter-free approaches are ultimately needed for understanding nuclear properties in terms of the fundamental interactions among the basic constituents of nuclear systems. In this talk, after a brief review of our recent studies on spin-polarized neutron matter, we discuss constraining the changing rate of the gravitational constant G and properties of (rapidly) rotating neutron stars by using a nuclear EOS partially constrained by the latest terrestrial nuclear laboratory data.

1 Introduction

Properties of matter under extreme pressure and density are of great interest in modern physics as they are closely related to numerous important nuclear phenomena in both the terrestrial laboratories and space. These properties depend on the interactions among the constituents of matter and are reflected in the equation of state (EOS) characterizing the medium. At high densities non-nucleonic degrees of freedom appear gradually due to the rapid rise of nucleon chemical potentials [1]. Among these particles are strange hyperons such as Λ^0 and Σ^- . At even higher densities matter is expected to undergo a phase transition to quark-gluon plasma [2]. Extracting the transition density from QCD lattice calculations is a formidable problem which is still presently unsolved. These complications introduce great challenges on our way to understanding behavior of matter in terms of interactions among its basic ingredients.

The EOS is important for many key processes in both nuclear physics and astrophysics. It has far-reaching consequences and governs dynamics of supernova explosions, formation of heavy elements, properties and structure of neutron stars, and the time variations of the gravitational constant G . Presently, the detailed knowledge of the EOS is still far from complete mainly due to the very poorly known density dependence of the nuclear symmetry energy, $E_{sym}(\rho)$. Different many-body theories yield, often, rather controversial predictions for the trend of $E_{sym}(\rho)$ and thus

the EOS. On the other hand, heavy-ion reactions at intermediate energies have already constrained significantly the density dependence of E_{sym} around nuclear saturation density, see e.g. [11, 13–16, 18]. Consequently, these constraints place also significant limits on the possible configurations of both static [12] and (rapidly) rotating [10] neutron stars, and the possible time variations of G [9]. In this report we review these findings. We also revisit our recent studies on spin-asymmetric neutron matter [8] with a particular emphasis on high densities.

2 Spin-polarized neutron matter: high-density regime

Studies of magnetic properties of dense matter are of great current interest in conjunction with studies of pulsars, which are believed to be rotating neutron stars with strong surface magnetic fields. Here we summarize briefly the results of our recent study on properties of spin-polarized pure neutron matter. For a detailed description of the calculation we refer the interested reader to Ref. [8] and the references therein. The computation is microscopic and treats the nucleons in the medium relativistically. The starting point of every microscopic calculation of nuclear structure and reactions is a realistic nucleon-nucleon (NN) free-space interaction. A realistic and quantitative model for the nuclear force with reasonable theoretical foundations is the one-boson-exchange (OBE) model [3]. Our standard framework consists of the Bonn B OBE potential together with the Dirac-Brueckner-Hartree-Fock (DBHF) approach to nuclear matter. A detailed description of applications of the DBHF method to isospin symmetric and asymmetric matter, and neutron-star properties can be found in Refs. [4–7].

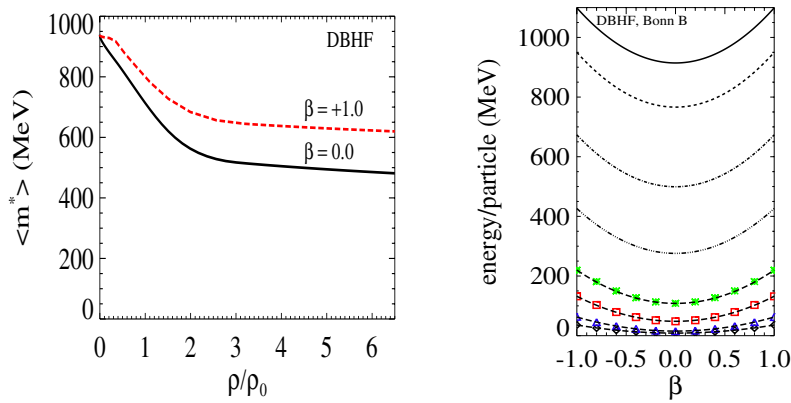


Figure 1. Left panel: Neutron effective masses used in the DBHF calculations of the EOS. The angular dependence is averaged out; Right panel: Average energy per particle at densities equal to 0.5, 1, 2, 3, 5, 7, 9, and 10 times ρ_0 (from lowest to highest curve).

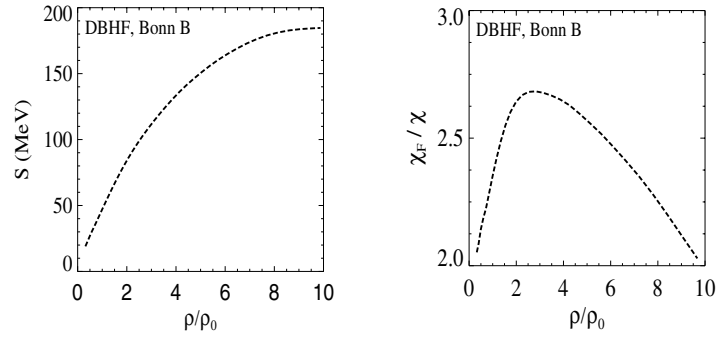


Figure 2. Left panel: Density dependence of the spin symmetry energy obtained with the DBHF model. Right panel: Density dependence of the ratio χ_F/χ .

To explore the possibility for a ferromagnetic transition the DBHF calculation has been extended to densities as high as $10\rho_0$ (with $\rho_0 \approx 0.16 \text{ fm}^{-3}$ the density of normal nuclear matter). Here we recall that the onset of ferromagnetic instabilities above a given density would imply that the energy-per-particle of a completely polarized state is lower than the one of unpolarized neutron matter. The same method as the one used in Ref. [7] has been applied to obtain the energy-per-particle where a self-consistent solution cannot be obtained (see Section III of Ref. [7] for details). The (angle-averaged) neutron effective masses for both the unpolarized and fully polarized case are shown in Fig. 1 (left panel) as a function of density. The spin-asymmetry parameter, $\beta = (\rho^\uparrow - \rho^\downarrow)/(\rho^\uparrow + \rho^\downarrow)$, quantifies the degree of asymmetry of the system. It can take values between -1 and +1 with 0 and the limits ± 1 corresponding to unpolarized and completely polarized matter respectively. ρ^\uparrow and ρ^\downarrow are the densities of neutrons with spins up/down. DBHF predictions for the average energy per particle are shown in Fig. 1 (right panel) at densities ranging from $\rho = 0.5\rho_0$ to $10\rho_0$. What we observe is best seen through the density dependence of spin-symmetry energy, $S(\rho)$, which is the difference between the energies of completely polarized and unpolarized neutron matter

$$S(\rho) = \bar{e}(\rho, \beta = 1) - \bar{e}(\rho, \beta = 0) \quad (1)$$

A negative sign of $S(\rho)$ would signify that a polarized system is more stable than unpolarized one. The spin-symmetry energy is shown as a function of density in Fig 2 (left panel). We see that at high density the energy shift between polarized and unpolarized matter continues to grow, but at a smaller rate, and eventually appear to saturate. For a detailed analysis of the observed behavior of $S(\rho)$ see Ref. [8]. Here we should mention that although the curvature of the spin-symmetry energy may suggest that ferromagnetic instabilities are in principle possible within the Dirac model, inspection of Fig. 2 reveals that such transition does not take place at least up to $10\rho_0$. Clearly, it would not be appropriate to explore even higher densities without

additional considerations, such as transition to a quark phase. In fact, even on the high side of the densities considered here, softening of the equation of state from additional degrees of freedom not included in the present model may be necessary in order to draw a more definite conclusion. In the right panel of Fig. 2 we show the density dependence of magnetic susceptibility, χ , in terms of χ_F , the magnetic susceptibility of a free Fermi gas. $\chi(\rho)$ is directly related to $S(\rho)$ through

$$\chi = \frac{\mu^2 \rho}{2S(\rho)}, \quad (2)$$

with μ the neutron magnetic moment. Clearly, similar observations apply to both left and right frames of Fig 2. (The magnetic susceptibility would show an infinite discontinuity, corresponding to a sign change of $S(\rho)$, in case of a ferromagnetic instability.)

In summary of this section, the EOSs we obtain with the DBHF model are generally rather repulsive at the larger densities. The energy of the unpolarized system (where all nn partial waves are allowed), grows rapidly at high density with the result that the energy difference between totally polarized and unpolarized neutron matter tends to slow down with density. This may be interpreted as a *precursor* of spin-separation instabilities, although no such transition is actually seen up to $10\rho_0$.

3 Constraining a possible time variation of the gravitational constant G with nuclear data from terrestrial laboratories

Testing the constancy of the gravitational constant G is a longstanding fundamental question in natural science. As first suggested by Jofré, Reisenegger and Fernández [20], Dirac's hypothesis [19] of a decreasing gravitational constant G with time due to the expansion of the Universe would induce changes in the composition of neutron stars, causing dissipation and internal heating. Eventually, neutron stars reach their quasi-stationary states where cooling, due to neutrino and photon emissions, balances the internal heating. The correlation of surface temperatures and radii of some old neutron stars may thus carry useful information about the rate of change of G . Using the density dependence of the nuclear symmetry energy, constrained by recent terrestrial laboratory data on isospin diffusion in heavy-ion reactions at intermediate energies [11, 13–16, 18], and the size of neutron skin in ^{208}Pb [21–24], within the *gravitochemical heating* formalism developed by Jofré et al. [20], we obtain an upper limit for the relative time variation $|\dot{G}/G|$ in the range $(4.5 - 21) \times 10^{-12} \text{yr}^{-1}$. In what follows we briefly review our calculation. For details see Ref. [9].

Recently a new method, called *gravitochemical heating* [20], has been introduced to constrain a hypothetical time variation in G , most frequently expressed as $|\dot{G}/G|$. In Ref. [20] the authors suggested that such a variation of the gravitational constant would perturb the internal composition of a neutron star, producing entropy which is partially released through neutrino emission, while a similar fraction

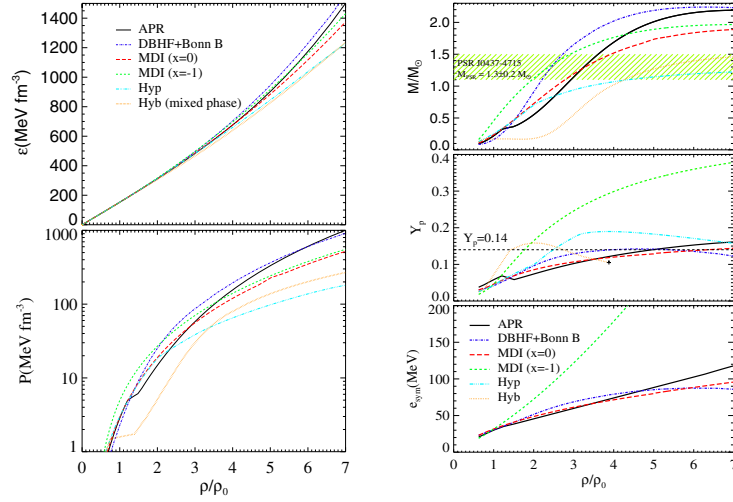


Figure 3. Left panel: Equation of state of stellar matter in β -equilibrium. The upper panel shows the total energy density and lower panel the pressure as function of the baryon number density (in units of ρ_0); Right panel: Neutron star mass, proton fraction, Y_p , and symmetry energy, e_{sym} . The upper frame displays the neutron star mass as a function of baryon number density. The middle frame shows the proton fraction and the lower frame the nuclear symmetry energy as a function of density. (Symmetry energy is shown for the nucleonic EOSs only.) The proton fraction curve of the Hyb EOS is terminated at the beginning of the quark phase. The termination point is denoted by a “cross” character.

is eventually radiated as thermal photons. A constraint on the time variation of G is achieved via a comparison of the predicted surface temperature with the available empirical value of an old neutron star [25]. The gravitochemical heating formalism is based on the results of Fernández and Reisenegger [26] (see also [27]) who demonstrated that internal heating could result from spin-down compression in a rotating neutron star (*rotochemical heating*). In both cases (gravito- and rotochemical heatings) predictions rely heavily on the equation of state (EOS) of stellar matter used to calculate the neutron star structure. Accordingly, detailed knowledge of the EOS is critical for setting a reliable constraint on the time variation of G .

Currently, theoretical predictions of the EOS of neutron-rich matter diverge widely mainly due to the uncertain density dependence of the nuclear symmetry energy. Consequently, to provide a stringent constraint on the time variation of G , one should attempt to reduce the uncertainty due to the $E_{sym}(\rho)$. Recently available nuclear reaction data allowed us to constrain significantly the density dependence of the symmetry energy mostly in the sub-saturation density region. While high energy radioactive beam facilities under construction will provide a great opportunity to pin down the high density behavior of the nuclear symmetry energy in the future. We apply the gravitochemical method with several EOSs describing matter of purely nucleonic ($npe\mu$) as wells as hyperonic and hybrid stars. Among the nu-

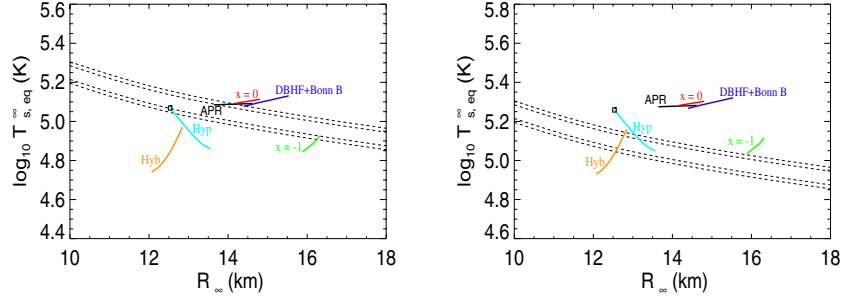


Figure 4. Left panel: Neutron star stationary surface temperature for stellar models satisfying the mass constraint by Hotan et al. [29]. The solid lines are the predictions versus the stellar radius for the considered neutron star sequences. Dashed lines correspond to the 68% and 90% confidence contours of the black-body fit of Kargaltsev et al. [25]. The value of $|\dot{G}/G| = 4.5 \times 10^{-12} \text{ yr}^{-1}$ is chosen so that predictions from the $x = 0$ EOS are just above the observational constraints; Right panel: Same as left panel but assuming $|\dot{G}/G| = 2.1 \times 10^{-11} \text{ yr}^{-1}$.

cleonic matter EOSs, we pay special attention to the one calculated with the MDI interaction [28]. The symmetry energy $E_{sym}(\rho)$ of the MDI EOS is constrained in the sub-saturation density region by the available nuclear laboratory data, while in the high-density region we assume a continuous density functional. The EOS of symmetric matter for the MDI interaction is constrained up to about five times the normal nuclear matter density by the available data on collective flow in relativistic heavy-ion reactions.

The EOSs applied with the gravitochemical heating method are shown in Fig. 3 (left panel). For description of these EOSs see Ref. [9] and references therein. The parameter x is introduced in the MDI interaction to reflect the largely uncertain density dependence of the $E_{sym}(\rho)$ as predicted by various many-body approaches. Since, as demonstrated in Refs. [11, 12], only equations of state with x between -1 and 0 have symmetry energies consistent with the isospin diffusion data and measurements of the skin thickness of ^{208}Rb , we thus consider only these two limiting cases. Fig. 3 (right panel) displays the neutron star mass (upper frame), the proton fraction (middle frame) and the nuclear symmetry energy (lower frame). The shaded region in the upper frame corresponds to the mass constraint by Hotan et al. [29].

As shown in Ref. [20] the stationary surface temperature is directly related to the relative changing rate of G via $T_s^\infty = \tilde{D} \left| \frac{\dot{G}}{G} \right|^{2/7}$, where the function \tilde{D} is a quantity depending only on the stellar model and the equation of state. The correlation of surface temperatures and radii of some old neutron stars may thus carry useful information about the changing rate of G . Using the constrained symmetry energy with $x = 0$ and $x = -1$ shown in Fig. 3 (right panel), within the gravitochemical heating formalism, as shown in Fig. 4, we obtained an upper limit of the relative changing

rate of G in the range of $(4.5 - 21) \times 10^{-12} \text{yr}^{-1}$. This is the best available estimate in the literature [9]. For a comparison, results with the EOS from recent DBHF calculations [4, 7] with the Bonn B OBE potential are also shown. Predictions with the DBHF+Bonn B EOS give roughly the same value for the stationary surface temperature, but at slightly larger neutron-star radius relative to the $x = 0$ EOS. For the effect of hyperonic and quark phases of matter on the possible time variations of G we refer the reader to our analysis in Ref. [9].

The gravitochemical heating mechanism has the potential to become a powerful tool for constraining gravitational physics. Since the method relies on the detailed neutron star structure, which, in turn, is determined by the EOS of stellar matter, further progress in our understanding of properties of dense, neutron-rich matter will make this approach more effective.

4 Constraining properties and structure of rapidly rotating neutron stars

Because of their strong gravitational binding neutron stars can rotate very fast [30]. The first millisecond pulsar PSR1937+214, spinning at $\nu = 641 \text{Hz}$ [31], was discovered in 1982, and during the next decade or so almost every year a new one was reported. In the recent years the situation changed considerably with the discovery of an anomalously large population of millisecond pulsars in globular clusters [2], where the density of stars is roughly 1000 times that in the field of the galaxy and which are therefore very favorable sites for formation of rapidly rotating neutron stars which have been spun up by the means of mass accretion from a binary companion. Presently more than 700 pulsars have been reported, and the detection rate is rather high.

In 2006 Hessels et al. [32] reported the discovery of a very rapid pulsar J1748-2446ad, rotating at $\nu = 716 \text{Hz}$ and thus breaking the previous record (of 641Hz). However, even this high rotational frequency is too low to affect the structure of neutron stars with masses above $1M_{\odot}$ [30]. Such pulsars belong to the slow-rotation regime since their frequencies are considerably lower than the Kepler (mass-shedding) frequency ν_k . (The mass-shedding, or Kepler, frequency is the highest possible frequency for a star before it starts to shed mass at the equator.) Neutron stars with masses above $1M_{\odot}$ enter the rapid-rotation regime if their rotational frequencies are higher than 1000Hz [30]. A recent report by Kaaret et al. [33] suggests that the X-ray transient XTE J1739-285 contains the most rapid pulsar ever detected rotating at $\nu = 1122 \text{Hz}$. This discovery has reawakened the interest in building models of rapidly rotating neutron stars [30].

Applying several nucleonic equations of state (see previous section) and the *RNS** code developed and made available to the public by Nikolaos Stergioulas [34,35], we construct one-parameter 2-D stationary configurations of rapidly

* Thanks to Nikolaos Stergioulas the *RNS* code is available as a public domain program at <http://www.gravity.phys.uwm.edu/rns/>

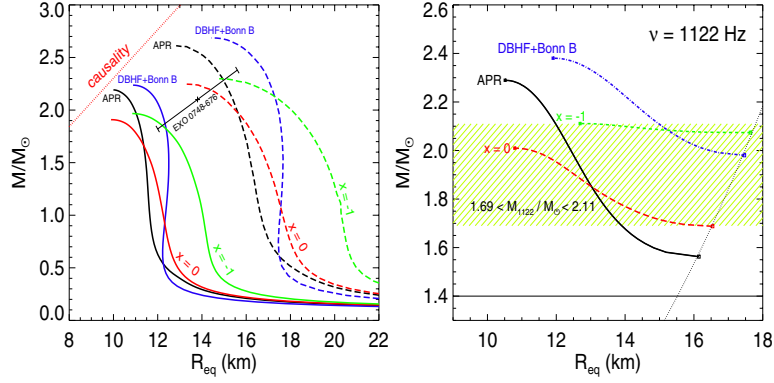


Figure 5. Left panel: Mass-radius relation. Both static (solid lines) and Keplerian (broken lines) sequences are shown. The $1 - \sigma$ error bar corresponds to the measurement of the mass and radius of EXO 0748-676 [36]; Right panel: Gravitational mass versus circumferential radius for neutron stars rotating at $\nu = 1122 Hz$.

rotating neutron stars (for details see Ref. [10]). The computation solves the hydrostatic and Einstein field equations for mass distributions rotating rigidly under the assumptions of stationary and axial symmetry about the rotational axis, and reflection symmetry about the equatorial plane.

The effect of ultra-fast rotation at the Kepler (mass-shedding) frequency is examined in the left panel of Fig. 5 (see also Table 1) where the stellar gravitational mass is given as a function of the *equatorial* radius. Predictions are shown for both static (non-rotating) and rapidly rotating stars. We observe that the total gravitational mass supported by a given EOS is increased by rotation up to 17% (see Ref. [10]). At the same time, the circumferential radius is increased by several kilometers while the polar radius (not shown here) is decreased by several kilometers, leading to an overall oblate shape of the rotating star.

Models of neutron stars rotating at $1122 Hz$ [33] are shown in Fig. 5 (right panel). Stability with respect to the mass-shedding from equator implies that at a

Table 1. Maximum-mass rapidly rotating models at the Kepler frequency $\nu = \nu_k$.

EOS	$M_{max}(M_{\odot})$	Increase (%)	$\epsilon_c (\times 10^{15} g cm^{-3})$	$\nu_k (Hz)$
MDI($x=0$)	2.25	15	2.59	1742
APR	2.61	17	2.53	1963
MDI($x=-1$)	2.30	14	2.21	1512
DBHF+Bonn B	2.69	17	2.06	1685

The first column identifies the equation of state. The remaining columns exhibit the following quantities for the maximally rotating models with maximum gravitational mass: gravitational mass; its percentage increase over the maximum gravitational mass of static models; central mass energy density; maximum rotational frequency.

given gravitational mass the equatorial radius R_{eq} should be smaller than R_{eq}^{max} corresponding to the Keplerian limit [30]. On the other hand, the stellar sequences are terminate at R_{eq}^{min} where the star becomes unstable against axial-symmetric perturbations. In Fig. 5 (right panel) we observe that the range of the allowed masses supported by a given EOS for rapidly rotating neutron stars becomes narrower than the one of static configurations. This effect becomes stronger with increasing frequency and depends upon the EOS. Since predictions from the $x = 0$ and $x = -1$ EOSs represents the limits of the neutron star models consistent with the nuclear data from terrestrial laboratories, we conclude that the mass of the neutron star in XTE J1739-285 is between 1.7 and $2.1M_{\odot}$.

5 Summary

We have presented an overview of our recent studies of effective interactions in dense neutron-rich matter and their applications to problems with astrophysical significance. The DBHF calculation of properties of spin-polarized neutron matter has been extended to high densities. Although no transition to a ferromagnetic phase is actually seen up to $10\rho_0$, the observed behavior of the spin-symmetry energy suggests that such transition may be possible at much higher densities. Applying the gravitochemical heating formalism developed by Jofre et al. [20] and the EOS with constrained symmetry energy, we have provided a limit on the possible time variation of the gravitational constant G in the range $(4.5 - 21) \times 10^{-12} yr^{-1}$. Our findings also allowed us to constrain the mass of the neutron star in XTE J1739-285 to be between 1.7 and $2.1M_{\odot}$.

In closing our discussion we would like to emphasize that further progress of our understanding of properties of dense matter can be achieved through coherent efforts of experiment, theory/modeling, and astrophysical observations.

Acknowledgments

We would like to thank Rodrigo Fernández and Andreas Reisenegger for helpful discussions and assistance with the numerics of the gravitochemical heating method. We also thank Fiorella Burgio for providing the hyperonic and hybrid EOSs and Wei-Zhou Jiang for helpful discussions. The work of Plamen G. Krastev, Bao-An Li and Aaron Worley was supported by the National Science Foundation under Grant No. PHY0652548 and the Research Corporation under Award No. 7123. The work of Francesca Sammarruca was supported by the U.S. Department of Energy under grant number DE-FG02-03ER41270.

References

1. M. Baldo, G. F. Burgio and H. -J. Schulze, Phys. Rev. C **61**, 055801 (2000).

2. F. Weber, *Pulsars as Astrophysical Laboratories for Nuclear and Particle Physics*, Bristol, Great Britan: IOP Publishing (1999).
3. R. Machleidt, *Adv. Nucl. Phys.* **19**, 189 (1989).
4. D. Alonso and F. Sammarruca, *Phys. Rev. C* **67**, 054301 (2003).
5. F. Sammarruca, W. Barredo and P. Krastev, *Phys. Rev. C* **71**, 064306 (2005).
6. F. Sammarruca and P. Krastev, *Phys. Rev. C* **73**, 014001 (2006).
7. P. G. Krastev and F. Sammarruca, *Phys. Rev. C* **74**, 025808 (2006).
8. F. Sammarruca and P. G. Krastev *Phys. Rev. C* **75**, 034315 (2007).
9. P. G. Krastev and B. A. Li, *Phys. Rev. C* (submitted); arXiv:nucl-th/0702080.
10. P. G. Krastev, B. A. Li and A. Worley, *ApJ* (submitted); arXiv:0709.3621 [astro-ph].
11. B. A. Li and L. W. Chen, *Phys. Rev. C* **72**, 064611 (2005).
12. B. A. Li and A. W. Steiner, *Phys. Lett. B* **642**, 436 (2006).
13. L. Shi and P. Danielewicz, *Phys. Rev. C* **68**, 064604 (2003).
14. M.B. Tsang et al., *Phys. Rev. Lett.* **92**, 062701 (2004).
15. L. W. Chen, C. M. Ko and B. A. Li, *Phys. Rev. Lett.* **94**, 032701 (2005).
16. A. W. Steiner and B. A. Li, *Phys. Rev. C* **72**, 041601 (2005).
17. B. A. Li and L. W. Chen, *Phys. Rev. C* **72**, 064611 (2005).
18. L. W. Chen, C. M. Ko and B. A. Li, *Phys. Rev. C* **72**, 064309 (2005).
19. P. A. M. Dirac, *Nature* **139**, 323 (1937).
20. P. Jofre, A. Reisenegger and R. Fernandez, *Phys. Rev. Lett.* **97**, 131102 (2006).
21. A. W. Steiner, M. Prakash, J. M. Lattimer and P. J. Ellis, *Phys. Rept.* **411**, 325 (2005).
22. C. J. Horowitz and J. Piekarewicz, *Phys. Rev. Lett.* **86**, 5647 (2001).
23. C. J. Horowitz and J. Piekarewicz, *Phys. Rev. C* **66**, 055803 (2002).
24. B. G. Tod-Rutel and J. Piekarewicz, *Phys. Rev. Lett.* **95**, 122501 (2005).
25. O. Kargaltsev, G. G. Pavlov and R. W. Romani, *Astrophys. J.* **602**, 327 (2004).
26. R. Fernandez and A. Reisenegger, *Astrophys. J.* **625**, 291 (2005).
27. A. Reisenegger, *Astrophys. J.* **442**, 749 (1995).
28. C. B. Das, S. D. Gupta, C. Gale and B. A. Li, *Phys. Rev. C* **67**, 034611 (2003).
29. A. W. Hotan, M. Bailes and S. M. Ord, *Mon. Not. R. Astron. Soc.* **369**, 15021520 (2006).
30. M. Bejger, P. Haensel, and J. L. Zdunik, *A&A*, 464, L49 (2007).
31. D. C. Backer, S. R. Kulkarni, C. Heiles, et al., *Nature*, 300, 615 (1982).
32. J. W. T. Hessels, S. M. Ransom, I. H. Stairs, et al., *Science*, 311, 1901 (2006).
33. P. Kaaret, J. Prieskorn, J. J. M. in't Zand, et al. *Astrophys. J.* **657**, L97 (2007).
34. N. Stergioulas, *Living Rev. Rel.*, 6, 3 (2003).
35. N. Stergioulas and J. L. Friedman, *Astrophys. J.*, 444, 306 (1995).
36. F. Ozel, *Nature*, 441, 1115 (2006).